Materials & Design 253 (2025) 113940

Contents lists available at ScienceDirect

Materials & Design

journal homepage: www.elsevier.com/locate/matdes

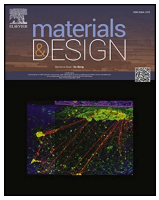

# Design and surface enhancement of ABS parts manufactured by Arburg plastic freeforming (APF) using chemical vapor treatment

Vaclav Janostik [a,*], Martin Cvek [b,*], Vladimir Pata [a], Vojtech Senkerik [a], Martin Ovsik [a]

[a] Department of Production Engineering, Faculty of Technology, Tomas Bata University in Zlin, Vavreckova 5669, 760 01 Zlin, Czech Republic
[b] Centre of Polymer Systems, University Institute, Tomas Bata University in Zlin, Trida T. Bati 5678, 760 01 Zlin, Czech Republic

ARTICLE INFO

*Keywords:*
Additive manufacturing
Freeforming
Chemical treatment
Surface design
Mechanical properties
Optimization

ABSTRACT

Additive manufacturing (AM) has become a key technology for fabricating highly customized products without the need for specific tools. Despite the benefits, this technology has some limitations, such as a poor surface finish of the products. Chemical treatment methods have been proven effective for the enhancement of surface finish. To this date, such treatments were applied to the objects manufactured by various AM methods, but there is no data available for the products manufactured by Arburg plastic freeforming (APF). The APF is a unique technique based on the deposition of tiny polymer droplets to build a final component directly from pellets. In this study, we investigate the effects of chemical treatment in hot acetone vapors on the surface roughness, (micro)mechanical properties, and optical and molecular changes of acrylonitrile butadiene styrene (ABS) samples produced by APF. The dynamics of the treatment process were studied as a function of exposure time to acetone vapors. The results showed that bulk mechanical properties were preserved, while significant changes occurred in the surface mechanics, specifically the indentation hardness. Along with the chemical treatment, the surface roughness exhibited nontrivial behavior but ultimately yielded a ~ 90 % reduction after 35 s, texture homogenization with the simultaneous improvement in gloss, from 2.2 to 45 GU, and surface aesthetics. The surface finishing process was very fast and easily scalable, offering valuable information for the design of ABS products in industrial applications.

## 1. Introduction

Arburg plastic freeforming (APF) technology, sometimes referred to as droplet deposition modeling, represents an innovative approach in jetting additive manufacturing (AM) that enables the production of functional three-dimensional (3D) objects from standard thermoplastic granulates. In the APF, the polymer granules are continuously fed through the hopper, melted in a heated plasticizing cylinder, and subsequently transported by a rotating screw to the pulsed nozzle tip. The special discharge unit controlled by the piezoactuator precisely applies the material in the form of droplets at a frequency of up to 200 droplets per second onto the build plate. The tiny polymer droplets fuse together, yielding a compact platform. As a result, complex and homogeneous objects can be produced using a layer-by-layer approach directly from the pellets without the need for injection molds and the standard prefabricated filaments [1–3]. Besides, compared to the conventional 3D printing technologies, such as fused deposition modeling (FDM) and selective laser sintering (SLS), the APF enables rapid prototyping, reducing production costs and offering new possibilities for the easy individualization of functional components with high quality and accuracy [2,4–6].

Recent studies focused on APF technology showed that the optimization of process parameters is crucial for achieving the compact structure and desired mechanical properties of the final products. The optimization typically involves a systematic interplay of thermal and geometric parameters affecting the shape of the droplets and thus increasing the filling density and mechanical properties [7]. The products fabricated by the APF technology were shown to exhibit higher densities, tensile, and flexural moduli when compared to those manufactured by fused filament fabrication (FFF) technology, close to the values achieved for the injection-molded parts [8].

An important area in the APF research is precision manufacturing, which aims to identify factors responsible for the good visual characteristics of the products. In this regard, it was found that the form factor is one of the most important parameters, together with layer thickness, nozzle, and build temperature, as well as overlap between raster and

* Corresponding authors.
*E-mail addresses:* vjanostik@utb.cz (V. Janostik), cvek@utb.cz (M. Cvek).

https://doi.org/10.1016/j.matdes.2025.113940
Received 21 January 2025; Received in revised form 19 March 2025; Accepted 9 April 2025
Available online 10 April 2025

filling and the raster angle [9]. The comparative analysis of three different AM techniques – FFF, SLS, and APF – showed that APF achieved higher dimensional accuracy despite a greater layer thickness (0.20 mm vs. 0.15 mm) for higher ISO sizes than FFF, represented by the modified Ghostprinters version of the Prusa i3. The SLS process represented by EOS Formiga P110 Velocis provided objects with a smoother surface with barely visible layers when compared to the FFF and APF, but showed poorer accuracy for smaller geometric elements, despite the use of a smaller layer thickness (0.10 mm), which was attributed to the adhesion of partially sintered particles and thermal effects [3].

The database of materials suitable for the APF includes a range of thermoplastic polymers, such as soft and elastic materials that cannot be efficiently processed using FFF technology [6,10]. The approved polymers for the APF are acrylonitrile butadiene styrene (ABS), polycarbonate (PC), thermoplastic urethane (TPU), and polypropylene (PP) [10], but also special polymers, such as polyethylenimine (PEI) [11], medical-grade poly(methyl methacrylate) (PMMA) [2], and biodegradable polylactic acid (PLA) [5,12].

In particular, ABS is a thermoplastic polymer commonly used for 3D printing [13], but is also recognized by Arburg as a suitable material for the APF. ABS represents a commercially important copolymer offering a good balance of impact and tensile properties, chemical and aging resistance, dimensional stability, and surface hardness [14]. These properties can be further tuned by varying the ratio of its comonomers; typical applications include protection and sports equipment, household appliances, and components for electronics, medical, and automotive industries [15].

As known, ABS products, especially those manufactured by AM technologies, typically require mechanical or chemical post-processing in order to tailor their surface properties and/or improve geometrical precision, aesthetic appearance, and other characteristics [16]. For instance, etching the surface of the ABS with sulfochromic acid is used in the electroplating to improve adhesion to the metallic coating [17]. In brief, exposure to sulfochromic acid yields the dissolution of the polybutadiene blocks, increasing the hydrophilicity on the surface of ABS and thus a better adhesion to metals. Besides the chemical changes, etching is accompanied by the formation of microporosity, which increases the interacting area for mechanical interlocking. Despite being an effective etching agent, sulfochromic acid is toxic and hazardous, which impels a need to minimize its consumption [18] or use more eco-friendly alternatives [17]. It was found that $MnO_2$-$H_3PO_4$-$H_2SO_4$ colloid in combination with ultrasound-assisted etching (UAE) significantly improved adhesive strength between the copper film and ABS (even more than etching in chromic acid) by creating more uniform cavities and a higher density of hydrophilic groups, despite the reduction in average surface roughness [19]. Similar effects and high efficiency of the etching process for the ABS surface can also be achieved by increasing/optimizing the temperature of the etching solutions [20]. Other strategies involve the use of high-energy irradiation, such as UV light [21] or pulsed laser activation [22], to modify the surface of the ABS. The main advantage of the radiation techniques is the possibility of fabricating well-defined patterns on the surface of ABS for high-resolution selective metallization.

In some applications, the opposite effects are needed, and organic solvents are used for removing surface (micro)porosity and reducing the risk of biological contamination. For instance, the surface of ABS parts manufactured by the FDM method was pre-treated with an acetone/water mixture in order to achieve a sealing effect, before being grafted with poly(ethylene glycol) (PEG) to improve water impermeability, hydrophilicity, and biocompatibility [23]. In another study, the ABS parts built by the FDM were exposed to cold acetone vapors, whose smoothing effects were investigated with respect to the different raster angles and different part orientations [24]. It was found that the orientation of objects along the X axis with a raster angle of 30° provided samples with superior mechanical properties and low surface roughness, while orientation in the Z axis resulted in longer build time and poor mechanical strength. The implications of vapor treatment were also examined for ABS samples produced by the FFF technology [25]. The authors used acetone and ethyl acetate, the latter representing a milder solvent, and their mixtures for conducting chemical vapor treatment of the referred samples. They found that the use of ethyl acetate required an exposure time of 30 min to achieve the desired enhancements in surface roughness; however, it did not interfere with the tensile strength of specimens, unlike acetone and its mixtures with ethyl acetate.

Considering the current literature, it becomes clear that surface finishing in chemical vapors has been investigated only on the ABS parts fabricated by FDM and FFF methods, but to the best of our knowledge, there are no publications addressing these problems on the objects manufactured using APF technology. For these reasons, this work aims to investigate the effects of hot acetone vapors on mechanical properties, particularly microhardness, and the surface morphology of ABS products manufactured by the APF. To gain deeper insights, the corresponding chemical changes of the ABS surface were studied using spectroscopy methods and correlated with the exposure time to acetone vapors. Moreover, the gloss examination, as a frequently overlooked characteristic, was performed, providing useful information about the optical and aesthetic properties. It is also noteworthy that acetone was selected as a suitable solvent due to its potent dissolution ability, allowing for smooth ABS surfaces in a very short time, making the procedure easily scalable and applicable in the industry. Due to the huge potential of the innovative APF technology and growing interest in the individualization of plastic components, we believe that present systematic investigations could open new avenues for the production and finishing operations of ABS parts integrated into the aforementioned applications.

## 2. Material and methods

### 2.1. Production of samples using APF

The samples were produced from the ABS pellets Terluran GP-35 (melt volume rate, MVR, of 34 $cm^3$/10 min at 220 °C) supplied by INEOS Styrolution (Germany) using the Freeformer 200-3X (Arburg, Germany), which is the first generation of the APF device, enabling the production of objects within a working space of 135 × 250 × 230 mm (Fig. 1**A**). The maximum temperature in a heated build chamber is up to 100 °C, while the temperature of the feeding unit can reach up to 300 °C, allowing for processing of high melting-point polymers. The diameter of the nozzle was 0.2 mm, which generally yields a higher thickness of the layer compared to the SLS method but does not necessarily translate into a lower quality of the product [3]. The ABS samples were designed as double-sided dumbbells for tensile testing (EN ISO 527, type 1A) and rectangular bars for impact testing (EN ISO-179), with thicknesses of 4 mm, thereby consisting of 20 layers. The build time of the tensile dumbbells was 62 min per sample, while the Charpy bars were produced within a build time of 23 min per sample. The series consisting of 5 samples of each type was produced using a single perimeter contour, 100 % infill, a 90 % overlap pattern, and a print frequency of 143 Hz. The slicing parameters are listed in Table 1, and visualized in Fig. 1**B**.

In the APF, a key process parameter is the drop aspect ratio (*DAR*), which is defined as the ratio between the width ($w_d$) and height ($h_d$) of the droplet extruded from the APF nozzle (Eq. (1)). The *DAR* is essential for achieving optimal structure and mechanical properties in the final product, and its proper calibration is critical for the dimensional accuracy and quality of the products.

$$DAR = \frac{w_d}{h_d} \tag{1}$$

The $w_d$ value depends on the volume of material flowing through the nozzle, which is influenced by the viscosity of the polymer (temperature) and the frequency of the piezoelectric actuator. The actuator

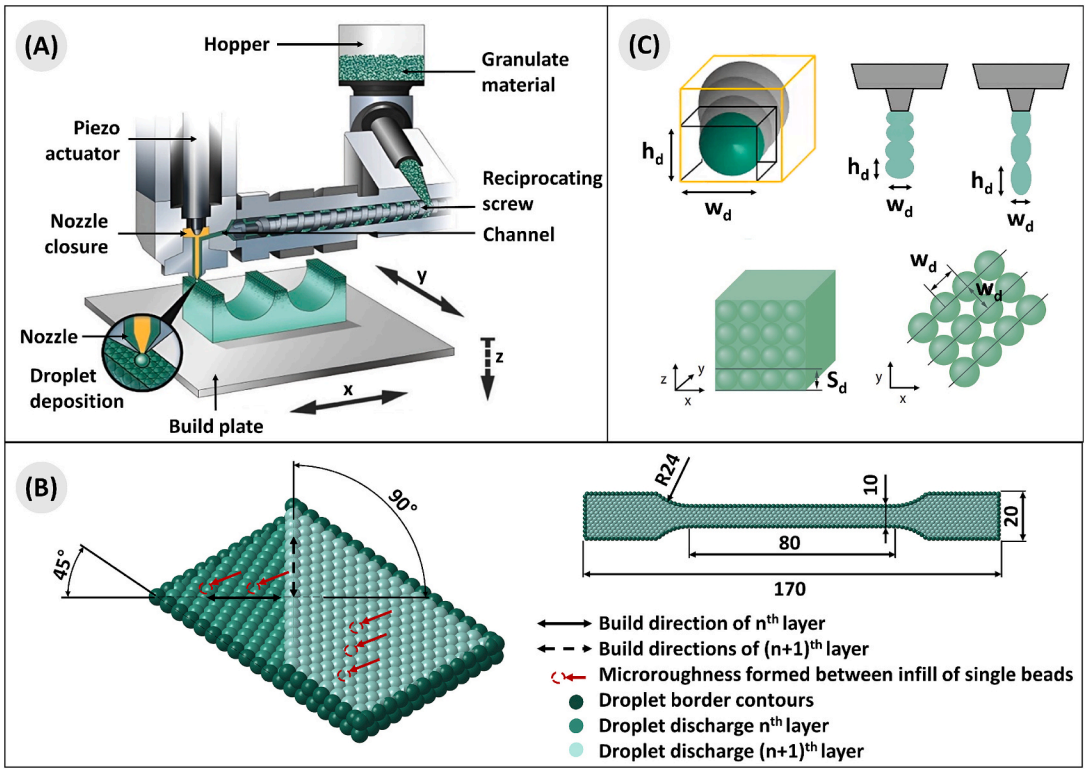


**Fig. 1.** (A) The scheme of the APF device/process. (B) Geometry of a specimen produced by APF including slicing schematics of raster angle orientations. (C) The tuning of the droplet geometry through the discharge rate per droplet and the rheological properties of the material, for a given nozzle. Test cubes are manufactured to precisely adjust the DAR value [26].

**Table 1**
A summary of the slicing parameters for the ABS constructs fabricated by APF.

| Design parameter | Applied value | Unit |
|---|---|---|
| Slice thickness | 0.2 | mm |
| Discharge | 70.0 | % |
| Number of border contours | 1.0 | – |
| Overlap contour | 50.0 | % |
| Self-supporting angle | 70.0 | % |
| Start angle | 45.0 | degree |
| Increment angle | 90.0 | degree |
| Filling degree | 100.0 | % |

**Table 2**
A summary of the process parameters for the ABS constructs fabricated by APF.

| Process parameter | Applied value | Unit |
|---|---|---|
| Drop aspect ratio, *DAR* | 1.32 | – |
| Nozzle temperature | 300 | °C |
| Build chamber temperature | 120 | °C |
| Melt speed | 20 | mm/s |
| Feed rate rapid mode | 250 | mm/s |
| Feed rate continuous extrusion, $h_S$ | 65 | mm/s |

controls the distance between individual nozzle positions, thereby determining the droplet width. The value of $h_d$ depends on the distance of the build platform during the deposition of droplets and determines the thickness of the layer [2]. Since the volume of the polymer flowing through the nozzle is influenced by material properties and process parameters, the *DAR* value has to be fine-tuned experimentally (Fig. 1**C**). A poor adjustment of the *DAR* is known to cause inadequate spacing between droplets, yielding underfilling and overfilling of the final object [6].

### 2.2. The setting of the APF process parameters

In additive manufacturing, proper setting of the process parameters is crucial for achieving the desired quality of the printed objects [27]. Herein, we applied the basic process parameters recommended by the manufacturer, including the nozzle and build chamber temperature, contouring speed, and feed rate in the rapid mode (Table 2). The same hatching strategy was also used for outlining the boundaries, overlap fill degree, and hatching orientation. It is worth mentioning that the hatching speed ($h_S$) represents the speed of the nozzle during layer filling and can be varied using three values (55, 65, and 75 mm/s). Such a range prevents the occurrence of significant defects, as excessive $h_S$ values lead to incomplete filling, affecting the density of the product, while lower $h_S$ values generally yield superior geometric accuracy but poor production efficiency. Finally, the aforementioned *DAR* value, which determines the spacing between the droplets, was experimentally set to 1.32 in order to prevent manufacturing defects. A lower *DAR* value can lead to significant time savings in production; but it is important to emphasize that shortening the overall build time ($t_B$) is not directly proportional to the $h_S$. Although a higher $h_S$ value may theoretically reduce the production time, the reality can be more complex due to potential impacts on the quality and integrity of the final product. Therefore, it is essential to carefully balance hatching speed with other production parameters, such as *DAR*, to achieve optimal results in terms of both time efficiency and product quality. Our APF settings allowed for the production of ABS constructs with not only the proper mechanical properties but also excellent visual characteristics.

### 2.3. Chemical treatment in acetone vapors

Considering the previous reports, two forms of chemical treatment of ABS surfaces can be distinguished, each offering specific advantages and disadvantages. The easiest method is based on the treatment in cold acetone vapors, where the ABS constructs are placed in a closed

container with a liquid acetone bath [28]. An alternative method is the treatment in hot acetone vapors, where the parts are exposed to vapors at an elevated temperature, which accelerates the kinetics of the process and more intensively smooths the surface. The latter process, however, might be more challenging to control [29]. Another commonly used technique is the direct application of acetone to the surface of ABS parts using a brush or another applicator, which allows for precise dosing of acetone and targeted treatment of specific areas [30]. Immersion treatment, where the ABS constructs are directly submerged in liquid acetone, significantly improves surface quality but can affect their dimensional stability [23]. In some cases, the immersion bath contains dispersed nanoparticles, resulting in their incorporation in the surface layers and simultaneous tuning of the surface properties [31].

For our experiments, having the industrial needs in mind, the chemical treatment in hot acetone vapors was considered. In detail, the ABS samples produced by the APF technique were placed in an acetone mist formed from an acetone bath (100 mL) poured into the etching chamber and heated to boiling point (b.p. of 56 °C) using a heating plate (MSH-A, Witeg, Germany) with magnetic stirring (120 rpm). The chamber was filled with acetone mist to 70–80 % of its volume, and this level was maintained consistently. The samples were treated in a fixed position using a mechanical holder within the etching chamber (Fig. 2), and the reaction time was set to 5, 10, 15, 20, 25, 30, and 35 s. Afterwards, the samples were conditioned for 48 h before further testing. The entire process took place in a controlled exhaust environment. The sample that was not exposed to the acetone vapors served as the reference throughout testing.

### 2.4. Microstructure analysis

The microstructure analysis was performed on the cross-section of freeze-fractured (liquid nitrogen) ABS samples. Due to unstable crack propagation in a brittle fracture, the ABS samples were also cut using a Flow Mach 500 (Waterjet, USA) waterjet system under a defined angle to study the changes near the surfaces. The abrasive waterjet (AWJ) cutting process involved the following parameters: machinability of 17.92, nozzle diameter of 0.3556 mm, mixing tube diameter of 1.016 mm, high water pressure of 410 MPa, and low water pressure of 130 MPa with an abrasive flow rate of 0.54 kg/min, using abrasive 80-mesh Alluvial garnet (Abranova, Czech Republic). The cutting speed was set to 7620 mm/min (40 % of the maximum speed), and the outline speed was set to 200 %.

The scanning electron microscopy (SEM) involved the Nova NanoSEM 450 device (FEI, Netherlands) equipped with a Schottky field-emission electron source and the Everhart-Thornley detector (ETD). Prior to the analysis, the samples were sputtered with a thin layer of gold using the SC760 coating device (Quorum Technologies, UK).

### 2.5. Tensile properties

The tensile properties of the ABS samples produced on a Freeformer 200-3X machine (Arburg, Germany) were determined following the technical standard EN ISO 527–1. The dumbbell samples were subjected to tensile testing using an M350-5 CT (Testometric, UK) device at a crosshead speed of 50 mm/min. The key mechanical parameters that were analyzed involved the ultimate tensile strength (*UTS*), Young's modulus ($E$), and relative elongation ($\varepsilon$). Among these parameters, the *UTS* was considered the most relevant from the perspective of applications [32].

### 2.6. Impact toughness

The impact toughness was determined using the Charpy method following the EN ISO 179–1 standard on the unnotched samples. A Zwick HIT50P pendulum impact tester (Zwick Roell, Germany) was used for characterization. During the testing, two main parameters were evaluated, such as impact toughness ($A_k$) and the energy required to break the sample ($W$).

### 2.7. Microindentation properties

The microindentation properties were measured using an MCT 2 instrumented hardness tester (CSM, Austria) equipped with a Vickers indenter with a pyramidal shape and a tip angle of 136°. The measurements were performed using the applied load of 1 N, a loading and unloading rate of 2 N/min, and a maximum load duration of 90 s. This method was carried out following the EN ISO 14577–1 standard, based on which the indentation hardness and indentation modulus were evaluated. The Oliver and Pharr method was used for data analysis, allowing for the precise determination of mechanical characteristics from indentation tests.

Indentation hardness ($H_{IT}$) characterizes the resistance of a material to permanent deformation or damage. The key parameters here are $F_{max}$, which is the maximum applied force, and $A_p$, which is the projected contact area (either theoretical or calibrated) [33–35]. The $H_{IT}$ can be obtained from the following equations:

$$H_{IT} = \frac{F_{max}}{A_p} \tag{2a}$$

$$A_p = 23.96 \cdot h_c^2 \tag{2b}$$

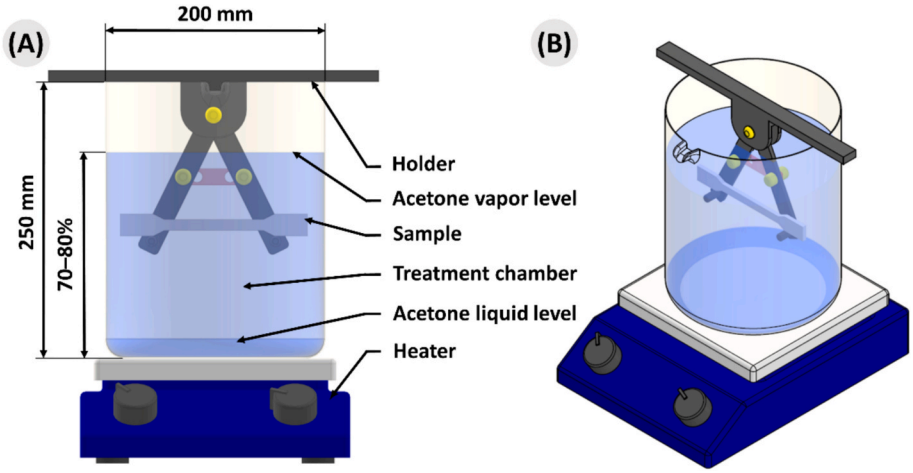


**Fig. 2.** The illustration, a side view (A) and a perspective (B), of the sample chemical treatment in acetone vapors.

where $h_c$ represents the contact depth. According to the aforementioned standard, the reduced modulus, $E_r$, is used to account for the fact that elastic displacements occur in both the indenter and the tested material. The indentation modulus of the tested material, $E_{IT}$, can be calculated from the $E_r$ using the following formula [33,34]:

$$E_{IT} = E^* \bullet \left(1 - \nu_s^2\right) \tag{3a}$$

$$E^* = \frac{1}{\frac{1}{E_r} - \frac{1-\nu_i^2}{E_i}} \tag{3b}$$

$$E_r = \frac{\sqrt{\pi}}{2 \cdot C \bullet \sqrt{A_p}} \tag{3c}$$

where $\nu_s$ and $\nu_i$ denote the Poisson's ratios and $E_r$ and $E_i$ the elastic moduli for the material of the sample and intender, respectively. In the case of ABS, the $\nu_s$ varies between 0.36 and 0.38, and a diamond intender is characterized by an $E_i$ of 1141 GPa and a $\nu_i$ of 0.07. The coefficient $C$ is the total compliance of the system dependent on the geometry of the intender [36].

### 2.8. Fourier-transform infrared (FTIR) spectroscopy

The FTIR spectra were recorded on an Alpha II (Bruker, Germany) spectrometer equipped with the ATR accessory fitted with a ZnSe crystal (a penetration depth of ~ 2 μm). The data was collected in the range from 4000 to 650 $cm^{-1}$ with a spectral resolution of 2 $cm^{-1}$, yielding 64 scans.

### 2.9. Analyses of surface roughness and surface texture

The surface roughness of the ABS samples manufactured by the APF method was analyzed using a Zygo NewView 8000 (Lambda Photometrics, UK) optical profilometer. The same device was also used for the assessment of the surface texture. For the non-contact surface roughness analysis, an area of 3000 × 3000 μm was selected and further divided into 50 longitudinal sections. The step size between individual sections was set to 60 μm, which was considered sufficient to capture relevant details of the surface texture. More specifically, such a step size was chosen to match the resolution capability of the APF technique and is adequate for the type and scale of the material texture used in industrial applications. This approach ensured that every detail of the surface was properly analyzed, and the roughness ($R_a$) values were representative of the overall surface quality of the material (Fig. 3**A**). Subsequent statistical analysis of the data confirmed a Gaussian distribution with random roughness values, as documented in the histogram (Fig. 3**B**). No extreme deviations were observed among the 50 sections. The average $R_a$ value from these measurements was then compared with the $S_a$ value, which represents the arithmetical mean height of a line extended to the analyzed surface [37], allowing for a detailed assessment of the surface quality of the examined material.

### 2.10. Gloss measurements

The specular gloss of the ABS surfaces was studied using the Proceq Zehntner ZGM 1120 (Screening Eagle Technologies, Switzerland) portable glossmeter, operating at a light incidence angle of 60°, following the ASTM D523 standard. This setup is considered suitable for surfaces exhibiting moderate gloss, i.e., from 10 to 70 GU (gloss units). Prior to measurements, surfaces were cleaned to remove any dust or contaminants that could interfere with accuracy. Calibration was performed against a certified reference standard, ensuring precision across readings. The device was positioned perpendicularly to the surface, and measurements were taken in single-click mode to ensure stability and consistency of data. The results were then transferred to a computer via Screening Eagle Workspace (Screening Eagle Technologies, Switzerland) software for storage and further analysis, providing reliable and reproducible gloss data.

## 3. Results and discussion

The APF process was configured to achieve high material density without voids, which is essential for the quality of the produced test specimens. The SEM analysis on the freeze-fractured areas revealed good contact between the adjacent layers and a compact microstructure of the ABS products (Fig. 4). Therefore, the manufactured specimens were considered relevant for the chemical treatment in acetone vapors and subsequent analyses.

### 3.1. Analysis of mechanical properties

To begin the analysis, we compared the mechanical parameters for the untreated (reference) ABS sample manufactured by the APF with those published in the relevant literature. The ultimate tensile strength, *UTS*, of our reference was 35.60 ± 1.13 MPa, which is a well-comparable value with those reported for the 3D-printed ABS using the FDM process, specifically 36.75 MPa [30] and 34.57 MPa [38]. Young's modulus equaled 2562 ± 131 MPa, which is close to the value for the injection-molded ABS and also similar to the ABS manufactured using APF (2309 ± 44 MPa) reported elsewhere [8]. These observations further corroborate that the APF process was optimized and the ABS samples exhibited high density and filling degree with a minimal number of air voids (Fig. 4).

Next, the dependence of the mechanical properties of the ABS samples manufactured by the APF technique on the chemical treatment time was investigated. As observed in Fig. 5**A and B**, the *UTS* and Young's modulus slightly decreased with the exposure time (by 9 % and 19 % after 35 s), suggesting a lower overall strength and material stiffness. In comparison, much more dramatic deterioration of the *UTS* (by 45 % and 49 %) was observed for the ABS immersed in the acetone and 1,2-dichloroethane for several minutes [30]. Contrary to the *UTS* and Young's modulus, the relative elongation markedly increased with the exposure time (from 4.7 % to 6.1 % after 35 s), indicating the improvement in the

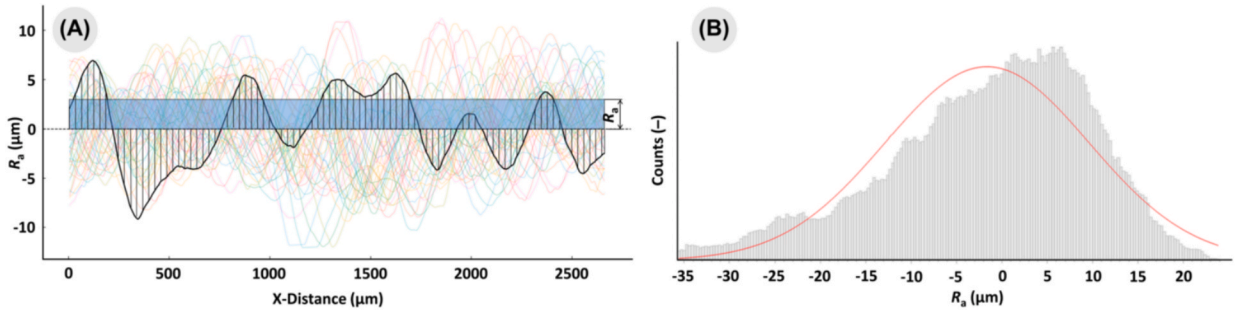


**Fig. 3.** The representative analysis of surface roughness: (A) the individual surface profiles of the ABS surface with the denoted region determining $R_a$ value and (B) the corresponding histogram of surface roughness distribution.

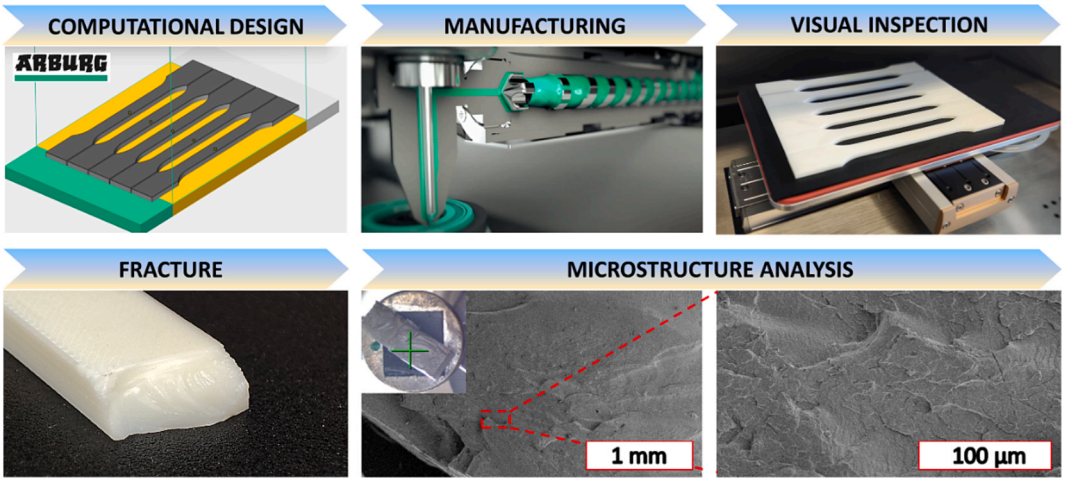


**Fig. 4.** The design, production, quality control, and SEM analysis of ABS samples manufactured by the APF technique.

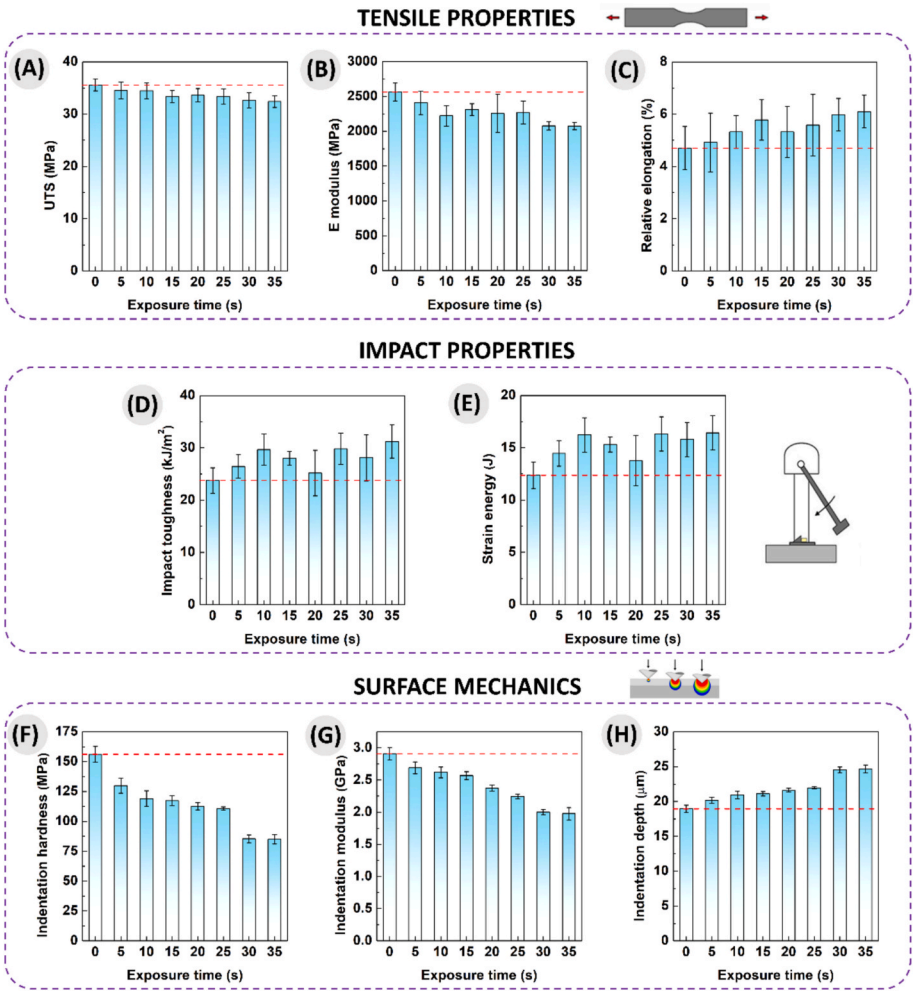


**Fig. 5.** Dependence of the (A) *UTS*, (B) Young's modulus, (C) relative elongation, (D) impact toughness, (E) maximum strain energy, (F) indentation hardness, (G) indentation modulus, and (H) indentation depth on the chemical treatment time.

ductility and the capability of stretching (Fig. 5**C**). The impact properties remained relatively unaffected, though a slight increase in the impact toughness, $A_K$, was indicative of a higher resistance to brittle fracture (Fig. 5**D and E**).

Expectedly, more significant changes were recorded for the surface properties. The indentation hardness, $H_{IT}$, as well as the indentation elastic modulus, $E_{IT}$, gradually decreased with the chemical treatment time (from 156.1 to 84.9 MPa and from 2.91 to 1.98 GPa, after 35 s), confirming the deterioration in the surface stiffness of the ABS (Fig. 5**F and G**). The reduced stiffness correlated with the indentation depth that followed the opposite trend and gradually increased as the material became softer and more easily penetrable.

### 3.2. Correlations between surface treatment and fracture behavior

Considering the experimental data (Fig. 5), it was concluded that acetone vapor treatment of the ABS manufactured by the APF influenced the fracture behavior of these parts. To gain better insights into the fracture mechanism, the microstructure changes near the surface were investigated using electron microscopy on the AWJ-cut samples. Fig. 6 details the evolution of cross-sectional morphology at different phases of the acetone treatment process. As seen in Fig. 6**A**, the untreated top surface layer consisted of evenly stacked droplets, formed by the action of the APF discharge unit. Despite a visible fusion of the microdroplets, the surface displayed distinct interdroplet boundaries, which during the uniaxial straining generated stress concentration, facilitating early crack initiation [39,40]. As a result, the samples exhibited a brittle fracture behavior, which correlates with the lower elongation at break in tensile tests [41]. After moderate exposure time (Fig. 6**B**), the ABS surface showed partial smoothing and visible homogenization of the outer layer. The boundaries between the adjacent microdroplets were still observable but less pronounced. These rearrangements decreased the likelihood of crack initiation from surface discontinuities, resulting in improved ductility and fracture toughness [42]. After prolonged hot acetone vapor exposure shown in Fig. 6**C**, the surface became highly homogenized and plasticized (Fig. 5**G**), without any visible geometrical discontinuities. The softened surface layer acted as a barrier to crack initiation by dissipating stress via plastic deformation, yielding remarkably improved elongation at break.

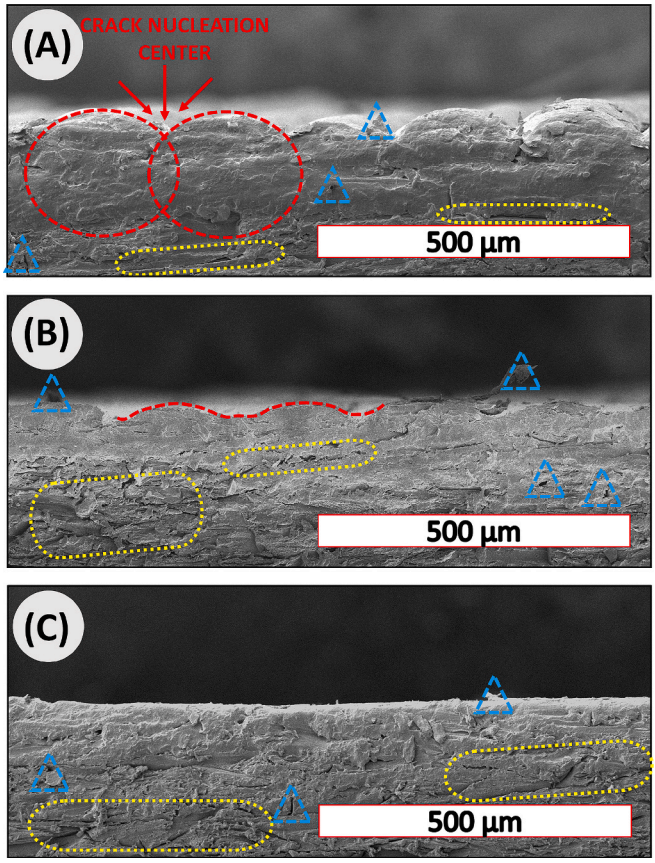


**Fig. 6.** SEM micrographs of the AWJ-cut ABS samples manufactured by the APF technique after exposure to hot acetone vapors for (A) 0, (B) 10, and (C) 35 s. Red dashed ellipses denote the individual microdroplets and their boundary perceived as the crack nucleation center. The yellow dashed ovals indicate kerf wall irregularities caused by AWJ cutting [44]. The blue dashed triangles mark residual abrasive particles from the AWJ cutting process, unrelated to the bulk ABS microstructure and fracture behavior. (For interpretation of the references to color in this figure legend, the reader is referred to the web version of this article.)

Regarding the depth of acetone penetration, it was reported that even immersing the 3D-printed ABS into an acetone solution did not affect the existence of the air gaps between the printed layers (a depth of 0.2 mm) [43]. Due to the lack of cavities in our samples, a similar observation could not be performed, but it is believed that only the top surface layers were affected by the acetone treatment.

In conclusion, the mechanical and fractographic analyses suggested that the ABS samples underwent complex changes in their surface microstructure, most likely accompanied by chemical changes (investigated in Section 3.3). The results demonstrate that short chemical vapor treatment of the ABS parts produced by the APF technology had a significant effect on their mechanical properties, especially the surface properties. Such effects should be taken into deep consideration when manufacturing components for applications where the material must meet specific requirements.

### 3.3. Changes in the molecular structure

The FTIR spectroscopy in the ATR mode was conducted to support the assumption of molecular changes in the surface of the ABS parts manufactured by the APF technology after their exposure to acetone vapors (Fig. 7). The structure of the ABS forms a binary phase system; the dispersed rubbery phase is represented by polybutadiene (PB), and the continuous rigid phase by the poly(styrene-*co*-acrylonitrile) (SAN) copolymer [45]. A fraction of the SAN chains is grafted onto PB (SAN-g-PB), while the rest of this phase is considered as free SAN [46]. Taking the complexity of the ABS microstructure into consideration, the investigation was made to identify which phase was responsible for the changes in acetone vapors. The characteristic absorption bands of polystyrene (PS) were located at wavenumbers $> 3000$ cm$^{-1}$ due to aromatic C–H stretching, while the peaks at 2924 and 2851 cm$^{-1}$ corresponded to the existence of methylenes and aliphatic C–H. The intense peaks at 1601, 1492, and 1452 cm$^{-1}$ were assigned to the aromatic C=C stretching vibrations, and signals at around 761–755 and 699 cm$^{-1}$ represented the C–H out-of-plane bending vibration coming from the benzene ring [47,48]. All peaks related to the PS progressively changed with the treatment time in acetone vapors, indicating its chemical changes (Fig. 7**A, C, E**). The most representative signature for acrylonitrile units is the stretching vibration of nitrile groups (C≡N) at 2236 cm$^{-1}$. This peak, however, exhibited negligible changes (Fig. 7**B**), which was associated with a poor dissolution capability of acetonitrile in acetone [49]. In regards to the PB phase, the peaks at around 1030–900 cm$^{-1}$ representing the C–H deformation vibration in the PB molecules showed minor changes (Fig. 7**D**), indicating the parallel degradation in the butadiene rubbery phase [47]. Besides, the appearance of the new peaks observed at 1711 and 1221 cm$^{-1}$ was associated with the reaction of the unsaturated C=C bond and a possible formation of new carbonyl- [45] and epoxy-containing species [50]. Nevertheless, the degradation in the PB phase is usually associated with the significant color changes of the ABS product [45,51], which was not observed in our case. Overall, based on the FTIR results, it can be concluded that the degradation in the ABS occurred mainly in the free SAN phase due to the solubility of PS in acetone; however, the chemical changes in the PB units should not be ruled out.

### 3.4. Surface roughness and topology changes

Surface roughness and topology changes are key properties for determining the quality, functionality, and aesthetic appeal of ABS products. Chemical vapor treatment in acetone was found highly effective for improving the surface roughness of 3D-printed ABS parts. For instance, the FDM-printed ABS parts were immersed in an acetone solution, and the $R_a$ decreased from 185.4 µm to 57.6 µm (after 2 intervals, 5 s each) [43]. In another study, the FDM-printed parts treated in cold acetone vapors showed improved $R_a$ from 37.2 µm to 10.1 µm (after

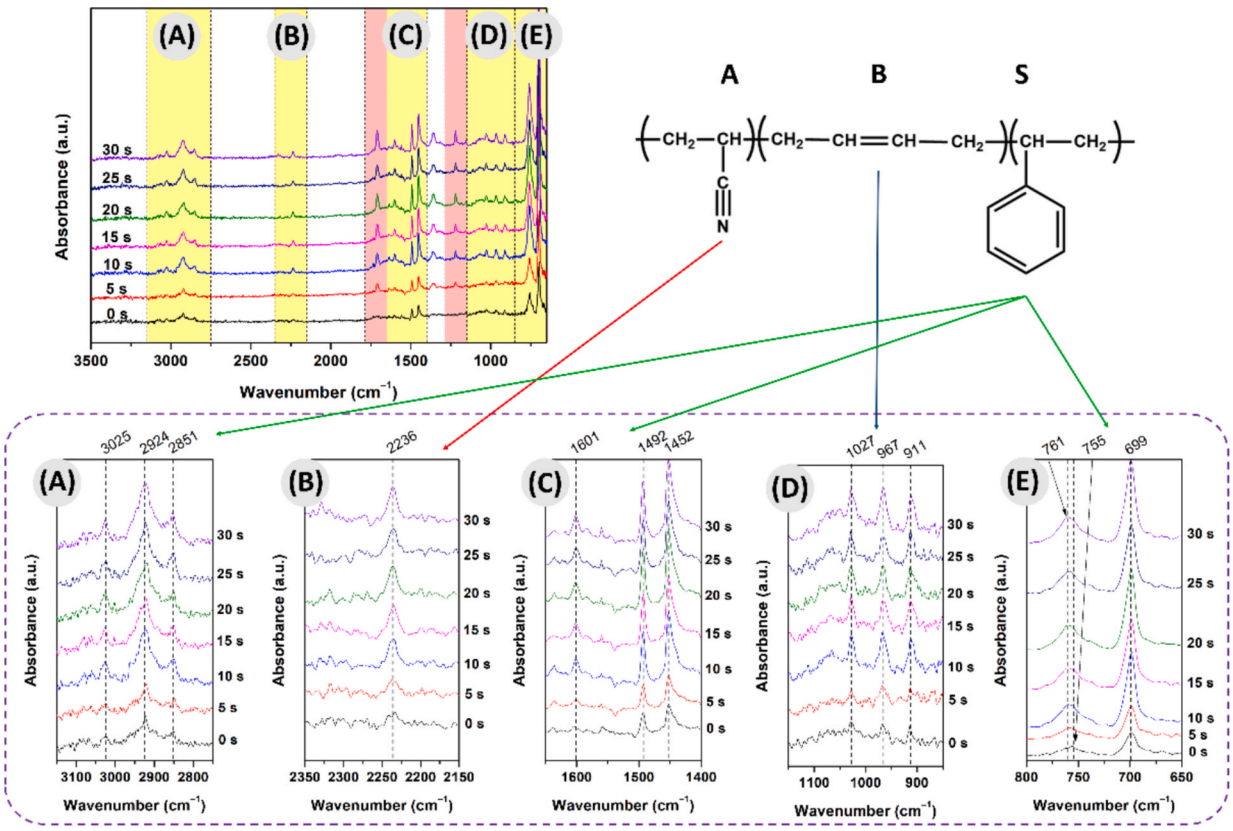


**Fig. 7.** The FTIR spectra of the ABS samples manufactured by the APF technique before and after their exposure to hot acetone vapors; the full-scale spectra with the magnified characteristic regions of ABS (denoted in yellow, A–E) and regions showing the appearance of new peaks (denoted in light red). (For interpretation of the references to color in this figure legend, the reader is referred to the web version of this article.)

45 min) [52]. For our samples manufactured using APF technology, the evolution of the relevant parameters, the $R_a$ and $S_a$, during the hot acetone vapor treatment is summarized in Table 3. As seen, the value of $S_a$ was generally higher than $R_a$ because it takes into consideration the roughness in a 3D space, while $R_a$ is measured along a single profile and is less sensitive to extreme peaks and valleys. However, both parameters exhibited similar trends with only slight differences, confirming their correlation in assessing surface roughness. As a consequence, both metrics can be considered reliable indicators of surface roughness.

When compared to the FDM-printed parts, the initial $R_a$ of our samples was significantly lower, most likely due to the unique concept of the APF technology utilizing the tiny microdroplets for building ABS products. The experimental results indicate that the time-dependent chemical finishing process can be divided into several phases, each reflecting specific changes in the roughness and texture of the material (Fig. 8). In the initial phase, within a five-second exposure to acetone vapor, a significant increase in surface roughness was observed. The $S_a$ roughness value increased from 5.654 to 8.901 μm, and the $R_a$ values from 5.302 to 8.564 μm. A possible reason behind this phenomenon is the formation of rough textures due to the intense chemical action of hot acetone vapors, which induced rapid erosions and the formation of coarse structures and protrusions. Subsequently, after five seconds of exposure, the surface roughness started to rapidly decrease; the $S_a$ value dropped to 1.653 μm and the $R_a$ value to 1.205 μm after twenty seconds of exposure, which was accompanied by a homogenization of the texture, better uniformity, and improved smoothness. The final phase can be denoted as the stabilization of surface roughness and reaching of the texture equilibrium, with the final $S_a$ and $R_a$ values of 0.801 and 0.571 μm achieved after thirty-five seconds of chemical treatment. These levels are in technical practice denoted as N6 grade of surface finish. Further exposure to acetone vapors no longer significantly affects the roughness or texture of the surface, which becomes uniformly smooth.

As mentioned, the chemical treatment process significantly impacted not only the roughness but also the texture of the surface. Fig. 9 depicts the evolution of surface texture for the ABS sample manufactured by APF with the exposure time to acetone vapors. The surface of the reference sample was densely covered with tiny spikes that, in the initial phase of chemical treatment, transformed into coarse, wavy structures (cf. Fig. 9**A and B**). With prolonged exposure to acetone vapors, the surface formed more pronounced linear textures that became thinner and less regular, subsequently a finely grained texture with fewer distinct lines (cf. Fig. 9**C, D, and E**). Subsequently, the surface texture was almost entirely obliterated, showing a good level of homogeneity and uniformity (Fig. 9**F**). In the final stages (cf. Fig. 9**G, and H**), the texture became consistently smooth and exhibited a stable, highly uniform finish, indicating that the equilibrium state had been achieved. The results demonstrate that careful optimization of exposure time to

**Table 3**
The surface roughness of ABS parts after different exposure times to acetone vapors.

| Time (s) | 0 | 5 | 10 | 15 | 20 | 25 | 30 | 35 |
|---|---|---|---|---|---|---|---|---|
| $S_a$ (μm) | 5.654 | 8.901 | 3.265 | 2.677 | 1.653 | 1.463 | 0.892 | 0.801 |
| $R_a$ (μm) | 5.302 | 8.564 | 3.043 | 2.135 | 1.205 | 1.098 | 0.753 | 0.571 |

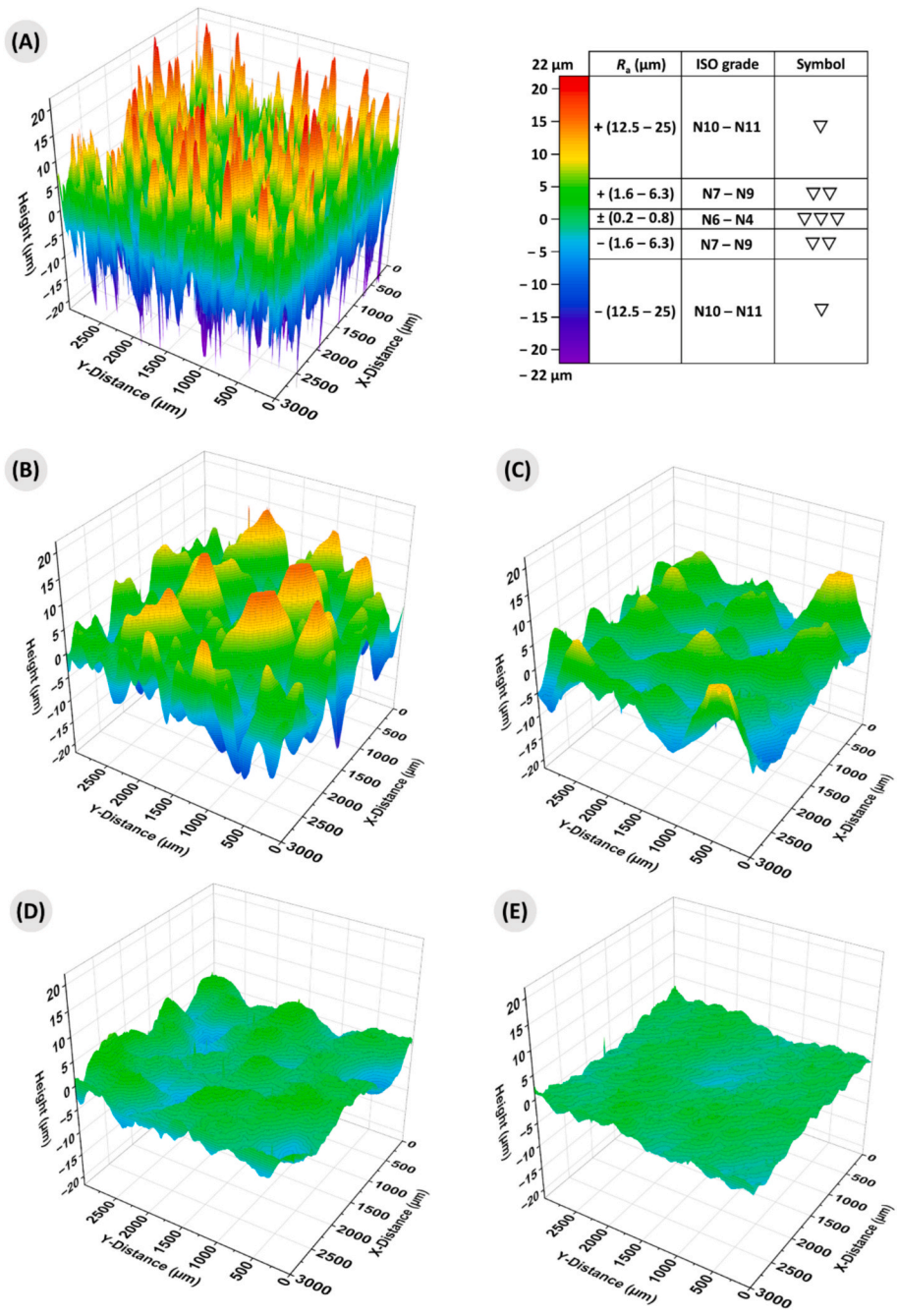


**Fig. 8.** 3D topographical surface analysis of ABS samples manufactured by the APF technique after different exposure times to hot acetone vapors; (A) 0, (B), 5, (C) 15, (D) 25, and (E) 35 s.

acetone vapors is crucial for achieving the desired control over the ABS surface finish in terms of surface roughness and texture uniformity. In practice, the presented methodology could be applied to mitigate the effects of thermal aging of ABS mold inserts, which is associated with increasing surface roughness [53].

### 3.5. Dynamics of the smoothing process

In the next phase, we aimed to develop a mathematical model to describe the dynamics of the smoothing process. The initial surface roughness value was not included in the mathematical model since it served as a reference point representing the original state of the surface before any exposure to acetone vapors. Since our study aimed to examine the dynamics of roughness changes caused by chemical treatment, we focused on the changes occurring after the initiation of the chemical process, i.e., within the exposure time, $t$, from 5 to 35 s. It was found that the dependence of the surface roughness ($R_a$) on the exposure time in hot acetone vapors followed the power-law equation:

$$R_a(\mu m) = 74.02 \times t(s)^{-1.348} \quad (4)$$

This model exhibited high accuracy with the correlation coefficient, $R^2$, of 0.991, allowing for a precise description of changes in surface roughness of ABS on the time of exposure to hot acetone vapors (Fig. 10**A**). Statistical tests confirmed the significance of all model parameters, the absence of multicollinearity, the homoscedasticity of the residuals, the normal distribution of the residuals, and the insignificance of autocorrelation. Therefore, the power-law model (Eq. (4) can provide reliable predictions for optimizing exposure time during surface

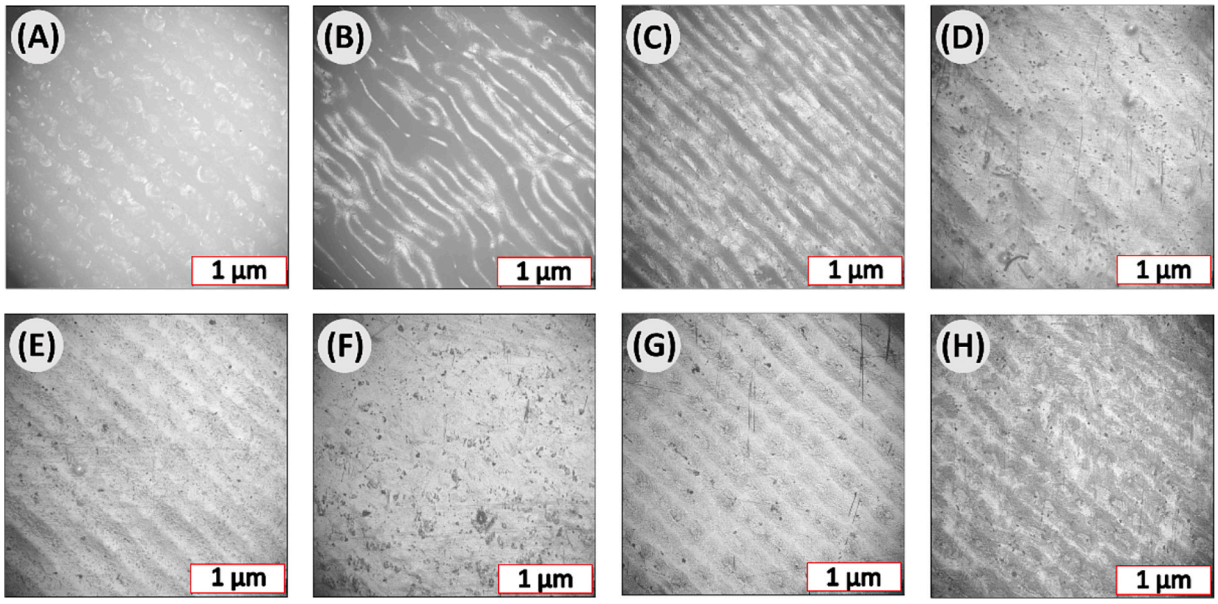


**Fig. 9.** Microscopic surface analysis of ABS samples manufactured by the APF technique after different exposure times to hot acetone vapors; (A) 0, (B) 5, (C) 10, (D) 15, (E) 20, (F) 25, (G) 30, and (H) 35 s.

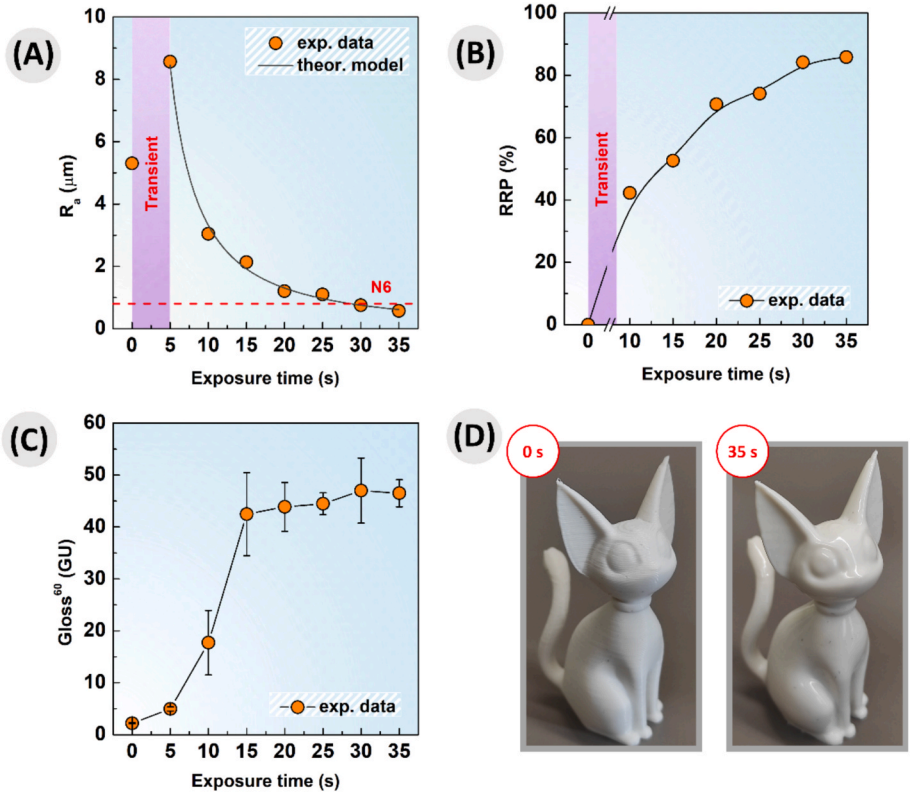


**Fig. 10.** (A) The surface roughness, expressed as $R_a$, (B) the RRP parameter, and (C) the gloss value as a function of the exposure time to hot acetone vapors. (D) The demonstration of the improved gloss on the complex macroscopic object before/after surface treatment.

finishing of ABS in hot acetone vapors.

Considering the fact that the smoothing mechanism is driven by the power-law model, the desired surface finish can be achieved very quickly. To further quantify the improvements, the roughness reduction parameter, *RRP*, was calculated according to the following equation:

$$RRP = \frac{S_a^i - S_a^f}{S_a^i} \times 100\% \quad (5)$$

where $S_a^i$ and $S_a^f$ denote the initial and final roughness, respectively [30]. As is obvious from Fig. 10**B**, the *RRP* markedly increased throughout the chemical treatment process, while reaching a value up to almost 90 % within 35 s. The efficiency of the process was compared with the chemical treatment of ABS parts in cold vapors of acetone and methyl ether ketone (MEK). In reported cases, the kinetics of the process were significantly slower, and the surface roughness decreased nearly linearly

with the exposure time; thus, the comparable $R_a$ values were achieved after 45 min, despite the comparable initial surface roughness [54]. Therefore, our finding showcases the superior efficiency of the hot vapor treatment.

### 3.6. Gloss and aesthetic characterization

Gloss is a defined physical property that, together with color and texture, gives the impression of the quality of the surface. A high level of gloss is often associated with good quality, and in some cases, it gives a more elegant impression to the product [55]. Fig. 10**C** displays the average $G^{60}$ values for the ABS parts as a function of the exposure time to hot acetone vapors. As seen, the sample manufactured by the APF possessed a low gloss (2.2 GU), most likely due to a relatively high initial roughness that affected the specular reflectance [56]. A rapid increase in $G^{60}$ was observed after the exposure time between 5 and 15 s, followed by the stabilization of its value around 45 GU, which is generally regarded as moderate glossiness. The overall trend showed an inverse relationship to the surface roughness, which is typical for homogeneous surfaces [57]. Finally, we demonstrate the remarkable improvement in gloss on the ABS object with a complex geometry (Fig. 10**D**). Initially, the surface was matte with visible lines from the APF printing process. After the chemical treatment, its texture became uniform with a glossy appearance, indicating a high level of aesthetic refinement.

## 4. Conclusions

In this work, the acetone vapor treatment was successfully adopted and optimized to enhance the surface finish of the ABS parts manufactured by the APF technique. The kinetics of the treatment were monitored, and its effects on mechanical properties, surface morphology, molecular changes, and optical properties in ABS were systematically investigated. The SEM analysis revealed the compact structure of the ABS with minimum air voids, suggesting that the APF process parameters, such as *DAR*, were optimized, which was also corroborated by the high *UTS* of the products (35.60 ± 1.13 MPa). Upon the treatment in vapors, the *UTS* and Young's modulus decreased minimally compared to the immersion methods. The relative elongation increased (from 4.7 % to 6.1 % after 35 s), while the surface stiffness in terms of the indentation hardness of the ABS gradually decreased with the treatment time (from 156.1 to 84.9 MPa, after 35 s), which was associated with the efficient reorganization of the topology and changes in the surface chemistry. A higher resistance to a brittle fracture was reflected in slightly improved impact properties. The surface stiffness in terms of the indentation hardness of the ABS gradually decreased with the treatment time (from 156.1 to 84.9 MPa, after 35 s). The FTIR spectroscopy revealed that the degradation of the ABS induced by acetone occurred in the SAN phase (mostly in the polystyrene units) as well as in butadiene, whereas the acrylonitrile units seemed chemically stable under the imposed experimental conditions. The profilometry revealed that time-dependent chemical treatment can be divided into three characteristic phases: at the beginning, the $R_a$ roughness increased from 5.302 to 8.564 μm, creating coarse, wavy structures, followed by its gradual decrease and changeover to a grainy texture; finally, the surface homogenized with the $R_a$ value of 0.571 μm. Compared to cold acetone vapor treatment, the kinetics of the presented approach followed a power-law mechanism and allowed for achieving the desired surface finish – almost a 90 % reduction in surface roughness – much faster, within 35 s. The final product also exhibited an excellent improvement in a $G^{60}$ value, from 2.2 to 45 GU. Considering the significant improvements in surface finish, retained mechanical properties, fast rate, and scalability of the operation, the presented treatment appears promising for the industrial finishing of ABS components manufactured by APF. Despite significant advancements in surface and mechanical properties, the long-term stability and durability of treated samples under different environmental conditions (e.g., UV exposure, humidity, and mechanical fatigue) were not investigated, which leaves space for future research endeavors.

## CRediT authorship contribution statement

**Vaclav Janostik:** Writing – review & editing, Writing – original draft, Visualization, Validation, Supervision, Resources, Project administration, Methodology, Investigation, Funding acquisition, Formal analysis, Data curation, Conceptualization. **Martin Cvek:** Writing – review & editing, Writing – original draft, Visualization, Validation, Supervision, Resources, Project administration, Methodology, Investigation, Funding acquisition, Formal analysis, Data curation, Conceptualization. **Vladimir Pata:** Validation, Methodology, Investigation, Formal analysis. **Vojtech Senkerik:** Validation, Investigation. **Martin Ovsik:** Validation, Investigation.

## Declaration of competing interest

The authors declare that they have no known competing financial interests or personal relationships that could have appeared to influence the work reported in this paper.

## Acknowledgement

M.C. acknowledges the project DKRVO (RP/CPS/2024-28/007) supported by the Ministry of Education, Youth and Sports of the Czech Republic.

## Data availability

Data will be made available on request.

## References

[1] H. Gaub, Customization of mass-produced parts by combining injection molding and additive manufacturing with Industry 4.0 technologies, Reinf. Plast. 60 (2016) 401–404, https://doi.org/10.1016/j.repl.2015.09.004.
[2] L. Hentschel, F. Kynast, S. Petersmann, C. Holzer, J. Gonzalez-Gutierrez, Processing conditions of a medical grade poly(methyl methacrylate) with the Arburg plastic freeforming additive manufacturing process, Polymers 12 (2020) 2677, https://doi.org/10.3390/polym12112677.
[3] P. Minetola, F. Calignano, M. Galati, Comparing geometric tolerance capabilities of additive manufacturing systems for polymers, Addit. Manuf. 32 (2020) 101103, https://doi.org/10.1016/j.addma.2020.101103.
[4] Q. Spiller, J. Fleischer, Additive manufacturing of metal components with the Arburg plastic freeforming process, CIRP Ann. 67 (2018) 225–228, https://doi.org/10.1016/j.cirp.2018.04.104.
[5] L.G. Engler, J.S. Crespo, N.M. Gately, I. Major, D.M. Devine, Process optimization for the 3D printing of PLA and HNT composites with Arburg plastic freeforming, J. Compos. Sci. 6 (2022) 309, https://doi.org/10.3390/jcs6100309.
[6] M. Mele, G. Campana, G. Fumelli, Environmental impact assessment of Arburg plastic freeforming additive manufacturing, Sustain. Prod. Consumption 28 (2021) 405–418, https://doi.org/10.1016/j.spc.2021.06.012.
[7] S. Charlon, J. Soulestin, Thermal and geometry impacts on the structure and mechanical properties of part produced by polymer additive manufacturing, J. Appl. Polym. Sci. 137 (2020) 49038, https://doi.org/10.1002/app.49038.
[8] P. Eyer, S. Enzler, A. Trauth, K.A. Weidenmann, Investigating the mechanical properties of polymer samples from different additive manufacturing processes using ultrasonic phase spectroscopy, 3D Print, Addit. Manuf. 11 (2024) e666–e674, https://doi.org/10.1089/3dp.2022.0148.
[9] A. Hirsch, F. Hecker, E. Moritzer, process parameter optimization to improve the mechanical properties of Arburg plastic freeformed components, Solid Freeform Fabr. Symp Proc., 2019.
[10] M. Neff, L. Pawelczyk, Resilient hard-soft combinations with plastic freeforming, Atzproduction Worldwide 6 (2019) 36–39, https://doi.org/10.1007/s38312-019-0017-8.
[11] D.M. Devine, ed., Polymer-based additive manufacturing, Springer International Publishing, Cham, (2019). https://doi.org/10.1007/978-3-030-24532-0.
[12] P. Stloukal, S. Pekařová, A. Kalendova, H. Mattausch, S. Laske, C. Holzer, L. Chitu, S. Bodner, G. Maier, M. Slouf, M. Koutny, Kinetics and mechanism of the biodegradation of PLA/clay nanocomposites during thermophilic phase of composting process, Waste Manag. 42 (2015) 31–40, https://doi.org/10.1016/j.wasman.2015.04.006.
[13] N. Dhakal, X. Wang, C. Espejo, A. Morina, N. Emami, Impact of processing defects on microstructure, surface quality, and tribological performance in 3D printed polymers, J. Mater. Res. Technol. 23 (2023) 1252–1272, https://doi.org/10.1016/j.jmrt.2023.01.086.

[14] Y.P. Shaik, N.K. Naidu, V.R. Yadavalli, M.R. Muthyala, The comparison of the mechanical characteristics of ABS using three different plastic production techniques, Open Access Library J. 10 (2023) 1–18, https://doi.org/10.4236/oalib.1110097.
[15] C.V. Pious, S. Thomas, Polymeric materials—structure, properties, and applications, in: Printing on Polymers, Elsevier, (2016) 21–39. https://doi.org/10.1016/B978-0-323-37468-2.00002-6.
[16] R.T. Mushtaq, Y. Wang, C. Bao, X. Chen, S. Anwar, S. Sharma, A.M. Khan, K. Sharma, Y.S. Bisht, M. Abbas, D. Kozak, V. Tropsa, Multi-objective optimization of laser polishing parameters for enhanced mechanical properties, sustainability, and surface finish of 3D-Printed industrial ABS polymers using response surface methodology (RSM), J. Mater. Res. Technol. 29 (2024) 3168–3184, https://doi.org/10.1016/j.jmrt.2024.02.023.
[17] R. Tao, L. Fatta, R. Melentiev, A.K. Tevtia, G. Lubineau, Contributions of chemical interactions and mechanical interlocking for the adhesion of electroplated copper to ABS in the Cr(VI) etching process, Int. J. Adhes. Adhes. 126 (2023) 103450, https://doi.org/10.1016/j.ijadhadh.2023.103450.
[18] R. Melentiev, R. Tao, G. Lubineau, Greener electrochemical plating of ABS polymer with unprecedented adhesion via hierarchical micro–nanotexturing, J. Mater. Res. Technol. 24 (2023) 3575–3587, https://doi.org/10.1016/j.jmrt.2023.04.001.
[19] Y. He, B. Li, Y. Shen, Z. Wang, Adhesion improvement of ABS resin by $MnO_2$-$H_3PO_4$-$H_2SO_4$ colloid with ultrasound-assisted etching treatment, J Adhes Sci Technol 36 (2022) 1883–1893, https://doi.org/10.1080/01694243.2021.1989225.
[20] X. Han, G. Wang, J. He, J. Guan, Y. He, Influence of temperature on the surface property of ABS resin in $KMnO_4$ etching solution, Surf. Interface Anal. 51 (2019) 177–183, https://doi.org/10.1002/sia.6560.
[21] L. Magallon Cacho, J.J. Pérez Bueno, Y. Meas Vong, G. Stremsdoerfer, F.J. Espinoza Beltran, J. Martinez Vega, Novel green process to modify ABS surface before its metallization: Optophysic treatment, J. Coat. Technol. Res. 12 (2015) 313–323, https://doi.org/10.1007/s11998-014-9632-5.
[22] J. Zhang, T. Zhou, L. Wen, Selective metallization induced by laser activation: fabricating metallized patterns on polymer via metal oxide composite, ACS Appl. Mater. Interfaces 9 (2017) 8996–9005, https://doi.org/10.1021/acsami.6b15828.
[23] E.J. McCullough, V.K. Yadavalli, Surface modification of fused deposition modeling ABS to enable rapid prototyping of biomedical microdevices, J. Mater. Process. Technol. 213 (2013) 947–954, https://doi.org/10.1016/j.jmatprotec.2012.12.015.
[24] A. Garg, A. Bhattacharya, A. Batish, Chemical vapor treatment of ABS parts built by FDM: analysis of surface finish and mechanical strength, Int. J. Adv. Manuf. Technol. 89 (2017) 2175–2191, https://doi.org/10.1007/s00170-016-9257-1.
[25] M. Mu, C.-Y. Ou, J. Wang, Y. Liu, Surface modification of prototypes in fused filament fabrication using chemical vapour smoothing, Addit. Manuf. 31 (2020) 100972, https://doi.org/10.1016/j.addma.2019.100972.
[26] Plastic Freeforming ADDITIVE MANUFACTURING. Kunststoffe International (2018). www.arburg.com/media/daten/other/fachartikel_kunststoffe_tr%C3%B6pfchen_im_millisekundentakt_11_2018_en.pdf.
[27] Y. Kayali, M. Ding, S. Hamdallah, S. Qi, R. Bibb, A. Gleadall, Effect of printing parameters on microscale geometry for 3D printed lattice structures, in: Mater Today Proc, Elsevier Ltd, 2022: pp. 31–37. https://doi.org/10.1016/j.matpr.2022.08.487.
[28] A. Colpani, A. Fiorentino, E. Ceretti, Characterization of chemical surface finishing with cold acetone vapours on ABS parts fabricated by FDM, Prod. Eng. 13 (2019) 437–447, https://doi.org/10.1007/s11740-019-00894-3.
[29] A. Lalehpour, C. Janeteas, A. Barari, Surface roughness of FDM parts after post-processing with acetone vapor bath smoothing process, Int. J. Adv. Manuf. Technol. 95 (2018) 1505–1520, https://doi.org/10.1007/s00170-017-1165-5.
[30] N. Jayanth, P. Senthil, C. Prakash, Effect of chemical treatment on tensile strength and surface roughness of 3D-printed ABS using the FDM process, Virtual Phys. Prototyp. 13 (2018) 155–163, https://doi.org/10.1080/17452759.2018.1449565.
[31] V. Francis, S. Garg, K.K. Saxena, P.K. Jain, J. Lade, D. Kumar, Effect of chemical and heat treatment on 3D printed parts: nanoparticles embedment approach, Adv. Mater. Processing Technol. 8 (2022) 2277–2288, https://doi.org/10.1080/2374068X.2022.2037876.
[32] V. Janostik, V. Senkerik, L. Manas, M. Stanek, M. Cvek, Injection-molded isotactic polypropylene colored with green transparent and opaque pigments, Int. J. Mol. Sci. 24 (2023) 9924, https://doi.org/10.3390/ijms24129924.
[33] W.C. Oliver, G.M. Pharr, Measurement of hardness and elastic modulus by instrumented indentation: advances in understanding and refinements to methodology, J. Mater. Res. 19 (2004) 3–20, https://doi.org/10.1557/jmr.2004.19.1.3.
[34] M. Ovsik, M. Manas, M. Stanek, A. Dockal, J. Vanek, A. Mizera, M. Adamek, P. Stoklasek, Polyamide surface layer nano-indentation and thermal properties modified by irradiation, Materials 13 (2020) 2915, https://doi.org/10.3390/ma13132915.
[35] D. Manas, A. Mizera, M. Manas, M. Ovsik, L. Hylova, S. Sehnalek, P. Stoklasek, Mechanical properties changes of irradiated thermoplastic elastomer, Polymers 10 (2018) 87, https://doi.org/10.3390/polym10010087.
[36] D. Chicot, M. Yetna N'Jock, E.S. Puchi-Cabrera, A. Iost, M.H. Staia, G. Louis, G. Bouscarrat, R. Aumaitre, A contact area function for Berkovich nanoindentation: application to hardness determination of a TiHfCN thin film, Thin Solid Films 558 (2014) 259–266, https://doi.org/10.1016/j.tsf.2014.02.044.
[37] M. Cvek, M. Mrlik, J. Sevcik, M. Sedlacik, Tailoring performance, damping, and surface properties of magnetorheological elastomers via particle-grafting technology, Polymers 10 (2018) 1411, https://doi.org/10.3390/polym10121411.
[38] K. Alvarez, R.F. Lagos, M. Aizpun, Investigating the influence of infill percentage on the mechanical properties of fused deposition modelled ABS parts, Ingeniería e Investigacion 36 (2016) 110–116, https://doi.org/10.15446/ing.investig.v36n3.56610.
[39] J. Allum, A. Gleadall, V.V. Silberschmidt, Fracture of 3D-printed polymers: crucial role of filament-scale geometric features, Eng. Fract. Mech. 224 (2020) 106818, https://doi.org/10.1016/j.engfracmech.2019.106818.
[40] B.N.J. Persson, Surface roughness-induced stress concentration, Tribol. Lett. 71 (2023), https://doi.org/10.1007/s11249-023-01741-4.
[41] M.R. Khosravani, S. Rezaei, H. Ruan, T. Reinicke, Fracture behavior of anisotropic 3D-printed parts: experiments and numerical simulations, J. Mater. Res. Technol. 19 (2022) 1260–1270, https://doi.org/10.1016/j.jmrt.2022.05.068.
[42] S. Yu, S. Park, K.T. Lee, J.Y. Hwang, S.H. Hong, T.J. Marrow, On the crack resistance and damage tolerance of 3D-printed nature-inspired hierarchical composite architecture, Nat. Commun. 15 (2024) 9532, https://doi.org/10.1038/s41467-024-53850-w.
[43] M.R. Khosravani, D. Anders, T. Reinicke, Effects of post-processing on the fracture behavior of surface-treated 3D-printed parts, CIRP J. Manuf. Sci. Technol. 46 (2023) 148–156, https://doi.org/10.1016/j.cirpj.2023.08.006.
[44] M. Muller, P. Valasek, M. Linda, V. Kolar, Research on water jet cutting of composites based on epoxy/microparticles from coconut shell, in: MATEC Web of Conf., EDP Sci. 244 (2018) 02001. https://doi.org/10.1051/matecconf/201824402001.
[45] A. Arostegui, M. Sarrionandia, J. Aurrekoetxea, I. Urrutibeascoa, Effect of dissolution-based recycling on the degradation and the mechanical properties of acrylonitrile–butadiene–styrene copolymer, Polym. Degrad. Stab. 91 (2006) 2768–2774, https://doi.org/10.1016/j.polymdegradstab.2006.03.019.
[46] A. Agirre, M. Aguirre, J.R. Leiza, Characterization of grafting properties of ABS latexes: ATR-FTIR vs NMR spectroscopy, Polymer 253 (2022) 124997, https://doi.org/10.1016/j.polymer.2022.124997.
[47] J. Li, F. Chen, L. Yang, L. Jiang, Y. Dan, FTIR analysis on aging characteristics of ABS/PC blend under UV-irradiation in air, Spectrochim. Acta, Part A 184 (2017) 361–367, https://doi.org/10.1016/j.saa.2017.04.075.
[48] J. Fang, Y. Xuan, Q. Li, Preparation of polystyrene spheres in different particle sizes and assembly of the PS colloidal crystals, Sci. China: Technol. Sci. 53 (2010) 3088–3093, https://doi.org/10.1007/s11431-010-4110-5.
[49] A. Yushkin, A. Basko, A. Balynin, M. Efimov, T. Lebedeva, A. Ilyasova, K. Pochivalov, A. Volkov, Effect of acetone as co-solvent on fabrication of polyacrylonitrile ultrafiltration membranes by non-solvent induced phase separation, Polymers 14 (2022) 4603, https://doi.org/10.3390/polym14214603.
[50] M.M.A. Nikje, A. Rafiee, M. Haghshenas, Epoxidation of polybutadiene using in situ generated dimethyl dioxirane (DMD) in the presence of tetra-n-butyl ammonium bromide, Des. Monomers Polym. 9 (2006) 293–303, https://doi.org/10.1163/156855506777351009.
[51] J.K. Kim, C.K. Kang, basic studies on recycling of ABS resin, Polym.-Plast. Technol. Eng. 34 (1995) 875–890, https://doi.org/10.1080/03602559508012182.
[52] C. Neff, M. Trapuzzano, N.B. Crane, Impact of vapor polishing on surface quality and mechanical properties of extruded ABS, Rapid Prototyp. J 24 (2018) 501–508, https://doi.org/10.1108/RPJ-03-2017-0039.
[53] A. Davoudinejad, M.R. Khosravani, D.B. Pedersen, G. Tosello, Influence of thermal ageing on the fracture and lifetime of additively manufactured mold inserts, Eng. Fail. Anal. 115 (2020) 104694, https://doi.org/10.1016/j.engfailanal.2020.104694.
[54] S. Nur, H. Mazlan, M.R. Alkahari, F.R. Ramli, N.A. Maidin, M.N. Sudin, A. R. Zolkaply, Surface finish and mechanical properties of FDM part after blow cold vapor treatment, J. Adv. Res. Fluid Mech. Therm. Sci. 48 (2018) 148–155.
[55] I. Arino, U. Kleist, L. Mattsson, M. Rigdahl, On the relation between surface texture and gloss of injection-molded pigmented plastics, Polym. Eng. Sci. 45 (2005) 1343–1356, https://doi.org/10.1002/pen.20393.
[56] S. Ignell, U. Kleist, M. Rigdahl, On the relations between color, gloss, and surface texture in injection-molded plastics, Color Res. Appl. 34 (2009) 291–298, https://doi.org/10.1002/col.20510.
[57] P. Sanmartin, B. Silva, B. Prieto, Effect of surface finish on roughness, color, and gloss of ornamental granites, J. Mater. Civ. Eng. 23 (2011) 1239–1248, https://doi.org/10.1061/(asce)mt.1943-5533.0000285.